Efficient fiber-to-chip grating coupler for micrometric SOI rib waveguides

C. Alonso-Ramos,[1,*] A. Ortega-Moñux,[1] I. Molina-Fernández,[1] P. Cheben,[2] L. Zavargo-Peche,[1] R. Halir[1]

[1]*Departamento Ingeniería de Comunicaciones, ETSI Telecomunicación, Universidad de Málaga, 29071 Málaga, Spain*

[2]*Institute for Microstructural Sciences, National Research Council of Canada, 1200 Montreal Rd., Bldg. M50, K1A 0R6 Ottawa, Ontario, Canada*

[*]*caar@ic.uma.es*

Abstract: Grating couplers are an efficient means for fiber to chip coupling, as they require no facet preparation and enable wafer scale testing. While grating couplers are commonly used in silicon wire waveguides, their application to micrometric silicon-on-insulator rib waveguides is complicated due to the presence of high-order Bloch modes. We study the Bloch modes behavior and their excitation determined by access waveguide design. The latter is implemented to enable single Bloch mode excitation. The use of a design process based on modal analysis is proposed. A grating coupler is proposed in silicon-on-insulator with 1.5μm thick silicon layer that achieves a coupling efficiency of 65.6% at 1.55μm. The structure, including interconnection waveguides, access waveguide and grating can be fabricated using a single lithography step.

OCIS codes: (230.3120) Integrated optics devices; (230.1950) Diffraction gratings; (230.7390) Waveguides, planar.

References and links

1. R. Soref, "The past, present, and future of silicon photonics," IEEE J. Sel. Top. Quantum Electron. **12**(6), 1678–1687 (2006).
2. L. Pavesi. and D. J. Lockwood, eds., *Silicon Photonics* (Springer, Berlin, 2004)
3. P. Cheben, R. Soref, D. Lockwood, and G. Reed, "Silicon Photonics," Adv. Opt. Technol. (2008) Article ID 510937, 2 pages, 2008. doi:10.1155/2008/510937
4. S. Janz, P. Dalacu, D. Delâge, A. Densmore, A. Lamontagne, B. Picard, M. Post, E. Schmid, J. Waldron, D. Xu, K.P. Yap, and W. Ye , "Microphotonic elements for integration on the silicon-on-insulator waveguide platform," IEEE J. Sel. Top. Quantum Electron. **12**(6), 1402–1415 (2006).
5. A. Sure, T. Dillon, J. Murakowski, C. Lin, D. Pustai, and D. Prather, "Fabrication and characterization of three-dimensional silicon tapers," Opt. Express **11**(26), 3555–3561 (2002).
6. V. Almeida, R. Panepucci, and M. Lipson, "Nanotaper for compact mode conversion," Opt. Lett. **28**(15), 1302–1304 (2003).
7. P. Cheben, D. Xu, S. Janz, and A. Densmore, "Subwavelength waveguide grating for mode conversion and light coupling in integrated optics," Opt. Express **14**(11), 4695–4702 (2006).
8. A. Delâge, S. Janz, D. Xu, D. Dalacu, B. Lamontagne, and A. Bogdanov, "Graded-index coupler for microphotonic SOI waveguides" in *Proc. of SPIE Photonics North 2004: Optical Components and Devices*, vol. 5577, pp. 204–212, 2004.
9. D. Taillaert, P. Bienstman, and R. Baets, "Compact efficient broadband grating coupler for silicon-on-insulator waveguides," Opt. Lett. **29**(23), 2749–2751 (2004).
10. D. Taillaert, W. Bogaerts, P. Bienstman, T. Krauss, P. Van Daele, I. Moerman, S. Verstuyft, K. De Mesel, and R. Baets, "An out-of-plane grating coupler for efficient butt-coupling between compact planar waveguides and single-mode fibers," IEEE J. Quantum Electron. **38**(7), 949–955 (2002).

#126348 - $15.00 USD Received 1 Apr 2010; revised 16 May 2010; accepted 19 May 2010; published 1 Jul 2010

11. G. Roelkens, D. Van Thourhout, and R. Baets, "High efficiency silicon-on-insulator grating coupler based on a poly-silicon overlay," Opt. Express **14**(24), 11622–11630 (2006).
12. F. Van Laere, G. Roelkens, M. Ayre, J. Schrauwen, D. Taillaert, D. Van Thourhout, T. Krauss, and R. Baets, "Compact and highly efficient grating couplers between optical fiber and nanophotonic waveguides," J. Lightwave Technol. **25**(1), 151–156 (2007).
13. P. Sanchis, J. Blasco, and J. Marti, "Study of high efficiency grating couplers for silicon-based horizontal slot waveguides," IEEE Photonics Technol. Lett. 20(12), 985–987 (2008).
14. G. Roelkens, D. Vermeulen, D. Van Thourhout, R. Baets, S. Brision, P. Lyan, P. Gautier, and J. Fedeli, "High efficiency diffractive grating couplers for interfacing a single mode optical fiber with a nanophotonic silicon-on-insulator waveguide circuit," Appl. Phys. Lett. **92** 131101 (2008).
15. B. Schmid, A. Petrov, and M. Eich, "Optimized grating coupler with fully etched slots," Opt. Express **17**(13), 11066–11076 (2009).
16. D. Xu, P. Cheben, D. Dalacu, A. Delâge, S. Janz, B. Lamontagne, M. Picard, and W. Ye, "Eliminating the birefringence in silicon-on-insulator ridge waveguides by use of cladding stress," Opt. Lett. 29(20), 2384–2386 (2004).
17. W. Ye, D. Xu, S. Janz, P. Cheben, M. Picard, B. Lamontagne, and N. Tarr, "Birefringence control using stress engineering in silicon-on-insulator (SOI) waveguides," J. Lightwave Technol. **23**(3), 1308–1318 (2005).
18. R. Halir, I. Molina-Fernández, A. Ortega-Moñux, J. Wangüemert-Pérez, D. Xu, P. Cheben, and S. Janz, "A design procedure for high-performance, rib-waveguide-based multimode interference couplers in silicon-on-insulator," J. Lightwave Technol. **26**(16), 2928–2936 (2008).
19. P. Trinh, S. Yegnanarayanan, F. Coppinger, and B. Jalali, "Silicon-on-insulator (SOI) phased-array wavelength multi/demultiplexer with extremely low polarization sensitivity," IEEE Photonics Technol. Lett. 9(7), 940–942 (1997).
20. P. Cheben, J. Schmid, A. Delâge, A. Densmore, S. Janz, B. Lamontagne, J. Lapointe, E. Post, P. Waldron, and D. Xu, "A high-resolution silicon-on-insulator arrayed waveguide grating microspectrometer with sub-micrometer aperture waveguides," Opt. Express 15(5), 2299–2306 (2007).
21. P. Cheben, A. Delâge, S. Janz, and D. Xu, *Echelle gratings and arrayed waveguide gratings for WDM and spectral analysis* in *Advances in Information Optics and Photonics*, A.T. Friberg and R. Dandliker, eds. (SPIE Press, Billingham, Washington, 2008), pp. 599–632.
22. K. Voigt, L. Zimmermann, G. Winzer, T. Mitze, J. Bruns, K. Petermann, B. Huttl, and C. Schubert, "Performance of 40-Gb/s DPSK demodulator in SOI-technology," IEEE Photonics Technol. Lett. 20(8), 614–616 (2008).
23. R. Soref, J. Schmidtchen, and K. Petermann, "Large single-mode rib waveguides in GeSi-Si and Si-on-SiO_2," IEEE J. Quantum Electron. 27(8), 1971–1974 (1991).
24. R. Halir, A. Ortega-Moñux, I. Molina-Fernández, J. Wangüemert-Pérez, P. Cheben, D. Xu, B. Lamontagne, and S. Janz, "Compact high performance multi-mode interference couplers in silicon-on-insulator," IEEE Photonics Technol. Lett. 21(21), 1600–1602 (2009).
25. R. Halir, P. Cheben, S. Janz, D. Xu, I. Molina-Fernández, and J. Wangüemert-Pérez, "Waveguide grating coupler with subwavelength microstructures," Opt. Lett. 34(9), 1408–1410 (2009).
26. K. Hill and G. Meltz, "Fiber Bragg grating technology fundamentals and overview," J. Lightwave Technol. 15(8), 1263–1276 (1997).
27. S. Helfert and R. Pregla, "Efficient analysis of periodic structures," J. Lightwave Technol. 16(9), 1694–1702 (1998).
28. T. Tamir and S. Peng, "Analysis and design of grating couplers," Appl. Phys. A-Mater. 14(3), 235–254 (1977).
29. M. Schnarrenberger, L. Zimmermann, T. Mitze, K. Voigt, J. Bruns, and K. Petermann, "Low loss star coupler concept for AWGs in rib waveguide technology," IEEE Photonics Technol. Lett. 18(23), 2469–2471 (2006).
30. Q. Cao, P. Lalanne, and J. Hugonin, "Stable and efficient Bloch-mode computational method for one-dimensional grating waveguides," J. Opt. Soc. Am. A 19(2), 335–338 (2002).
31. L. Zavargo-Peche, C. A. Alonso-Ramos, A. Ortega-Moñux, R. Halir, J. G. Wangüemert-Pérez, and I. Molina-Fernández, "A tool for automatic grating design," in *XVIII International Workshop Optical Waveguide Theory and Numerical Modeling (OWTNM 2009)*, 2009, p. 45.
32. A. Ortega-Moñux, I. Molina-Fernández, and J. Wangüemert-Pérez, "3D-Scalar Fourier eigenvector expansion method (Fourier-EEM) for analyzing optical waveguide discontinuities," Opt. Quantum Electron. 37(1), 213–228 (2005).

1. Introduction

Silicon photonics has undergone a remarkable development in the recent years. Silicon-on-insulator (SOI) offers important advantages; including high refractive index contrast that allows a high integration scale, and CMOS compatibility [1, 2, 3]. One of the challenges of the SOI platform is the mismatch, both in refractive index and mode size, between SOI waveguides

#126348 - $15.00 USD Received 1 Apr 2010; revised 16 May 2010; accepted 19 May 2010; published 1 Jul 2010

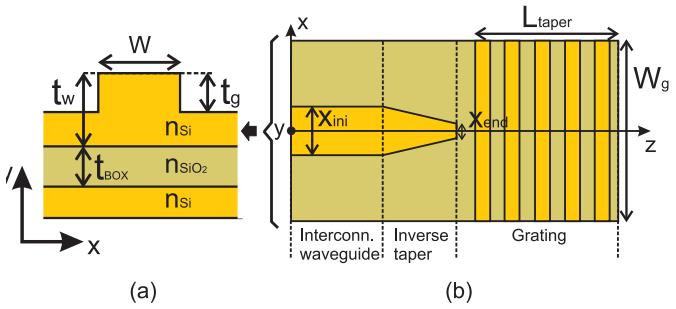

Fig. 1. (a) SOI Rib waveguide transverse geometry. (b) schematic top view of the coupler, including access waveguide, inverse taper and grating.

used in this technology and the standard optical fibers. Thus the development of efficient light injection and extraction structures is a key point in the success of this platform [4].

Various structures using light coupling through the chip facet have been proposed, including 3D tapers [5], inverse tapers [6], subwavelength waveguide grating couplers [7] or microlenses [8]. Another promising alternative is coupling light to the integrated circuit through the surface of the chip using a grating coupler [9, 10, 11, 12, 13, 14, 15]. As light can be injected and extracted at arbitrary location on the chip, wafer scale testing can be used and the need of antirreflection coatings or facet polishing is avoided, reducing associated packaging costs. Grating couplers also provide improved alignment tolerances and comparatively high coupling efficiency [9]. While these structures are narrowband compared to facet coupling, their typical bandwidth ($\sim$ 40nm), is adequate for a wide range of applications.

To the best of our knowledge, grating couplers have only been implemented in nanophotonic Si-wire waveguides but not in larger SOI rib waveguides. Although nanophotonic waveguides are a very promising technology that offers ultracompact integration capability, micrometric rib waveguides offers a series of advantages, including an improved polarization performance (lower birefringence and reduced polarization dependent loss) [16, 17], and bigger size that allows for standard i-line stepper lithography. Micrometric rib waveguides have reached a higher level of maturity and have demonstrated excellent performance implementing devices such as multimode interference couplers [18], arrayed waveguide grating wavelength multi/demultiplexers [19, 20, 21] or differential phase-shift keying (DPSK) demodulators [22]. Figure 1a shows the transversal geometry for a typical SOI micrometric rib waveguide. This waveguide rib geometry has been widely used in SOI, because it can be designed as single-moded by controlling rib dimensions [23]. Typical single-mode waveguide dimensions are $t_w = 1.5\mu$m, $W = 1.3\mu$m, and $t_g = 0.75\mu$m.

In this work a systematic procedure for designing efficient fiber-to-chip grating couplers for SOI rib waveguides of micrometric dimensions is proposed for the first time. The aim of the design is to maximize coupling efficiency considering two fabrication constraints:

- Standard fabrication process: Feature sizes should be larger than 0.5μm so that they can be realized with i-line stepper lithography.
- A single lithography and etch step to be used for the definition of the grating coupler, interconnecting waveguides and other photonic components, such as MMIs [24].

In Fig. 1b a schematic top view of the coupler device is shown, including the interconnection waveguide, an adiabatic taper (called hereafter excitation stage) and the grating.

This paper is organized as follows. In the next section some fundamental considerations for grating couplers will be reviewed. Section 3 is dedicated to Bloch modes supported by periodic

#126348 - $15.00 USD Received 1 Apr 2010; revised 16 May 2010; accepted 19 May 2010; published 1 Jul 2010

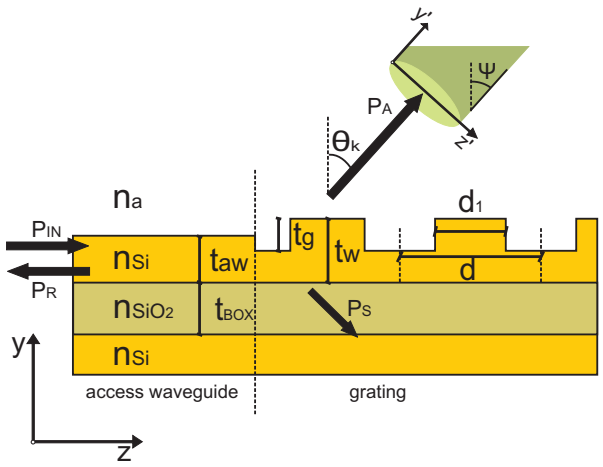

Fig. 2. Schematic view of a fiber-chip grating coupler.

structures in thick SOI waveguides, since the coupler design is greatly simplified using the Bloch mode representation. Consequences of the multimode behavior of the grating region will be examined. While the excitation of horizontal higher order modes is readily avoided using an adiabatic taper, the vertical higher order Bloch modes can exist in the grating region. Their analysis is a key aspect of this paper and will be discussed in section 4, where it will be shown that single-mode operation of a multimode grating can be achieved by judicious design of the excitation stage. In section 5 a systematic procedure for designing the two main components of the device, i.e. the excitation stage and the grating section is proposed. In section 6 device performance, including coupling efficiency, back reflection and radiation angle, is analyzed. Finally, conclusions are drawn.

2. Grating couplers

A grating coupler is a periodic structure connected to a waveguide in order to extract light from, or couple it to, a planar waveguide circuit. Ideally a grating coupler produces a single-beam of radiation efficiently coupled to the fundamental mode of the waveguide. This radiated power is typically collected using an optical fiber. Indeed, due to reciprocity, grating couplers can be used to extract light from the planar waveguide circuit and to inject light into it.

The grating width, W_g, is designed to optimize the coupling to fiber efficiency [9]. For a standard SMF-28 fiber, the optimum value for W_g is found to be 14.1μm. Subsequently, the design of the other parameters of the grating is carried out using a simplified two dimensional model [9].

Figure 2 shows a schematic 2D-view of a rectangular grating, including its geometrical parameters: the access waveguide height t_{aw}, the grating pitch d, the length of the non-etched slots d_1, and the etch depth t_g. Duty cycle is defined as $DC = d_1/d$.

The amount of power that is coupled into an optical fiber can be expressed as:

$$P_{\text{fiber}} = P_{IN}\eta_{\text{air}}\eta_{\text{fiber}}, \tag{1}$$

where P_{IN} is the power in the access waveguide and η_{air} and η_{fiber} are the fraction of the power in the access waveguide that is radiated to the air and the fraction of the air radiated power that is coupled to the fiber, respectively.

#126348 - $15.00 USD Received 1 Apr 2010; revised 16 May 2010; accepted 19 May 2010; published 1 Jul 2010

In order to maximize η_{fiber} both amplitude and phase of the radiated field and the optical fiber mode need to match.

The main factor limiting the coupling efficiency is the mismatch between the exponential radiated field in proximity of the grating and the Gaussian-like fundamental mode of the optical fiber. This field mismatch can be reduced using apodization [25].

While it may be desirable to use vertical (90°) coupling geometry, a small deviation angle ($\sim 10°$) from the vertical is usually chosen to avoid second order Bragg diffraction and thus reduce return loss [26].

3. Bloch modes

Bloch modes naturally appear as the solution of Maxwell's equations for periodic structures [15, 27]. These solutions can be expressed as

$$\vartheta(y,z) = \sum_k f_k(y) e^{-\Gamma_k z} = \vartheta(y,z+d) e^{-\Gamma_o d}, \tag{2}$$

where d is the structural pitch, k is the diffraction order and $f_k(y)$ is a function of the transversal coordinate y. The complex propagation constant Γ_k is defined by the Bloch theorem as

$$\Gamma_k = \alpha + j\beta_k = \alpha + j\left(\frac{2\pi}{\lambda} n_g + \frac{2\pi}{d} k\right) = \Gamma_o + j\frac{2\pi}{d} k, \tag{3}$$

where $\Gamma_o = \alpha + j\frac{2\pi}{\lambda} n_g$ is the complex propagation constant of the zeroth diffraction order, α accounts for the total radiation loss (air and substrate), and n_g is the effective index of the Bloch mode.

The calculation of the air radiation angles θ_k (Fig. 2) is straightforward from the phase matching equation

$$\theta_k \quad = \quad \arcsin\left(\frac{1}{n_a}(n_g + \frac{k\lambda}{d})\right). \tag{4}$$

Since θ_k must be a real number, only those diffraction orders that satisfy the following radiation condition will produce air radiation beams [28]:

$$-\frac{d}{\lambda}(n_a + n_g) < k < \frac{d}{\lambda}(n_a - n_g), \tag{5}$$

From Eq. (5) and taking into account that $n_g > n_a\,(n_a = 1)$ it is observed that only negative diffraction orders (i.e. $k < 0$) can radiate power into the air. It is also observed that for a fixed operating wavelength, the number of air radiation beams depends on the effective indexes of the Bloch modes (n_g) and the grating pitch (d). It can be shown that n_g mainly depends on the materials, the grating etch depth and the duty cycle, but is almost independent on the pitch [28]. Thus, a single air radiation beam can be obtained by properly choosing the grating pitch. This study is analogous for substrate radiation characteristics, just changing n_a by n_{SiO_2} in (4) and (5).

On the other hand, the number of Bloch modes supported by the grating depends on the materials and the substrate thickness (t_w). Since grating couplers fabricated in nanophotonic Si-wire waveguides ($t_w = 220$nm) typically operate in single-mode regime, coupling to a single air radiation beam is straightforward. Unfortunately, the situation is dramatically different for gratings implemented in thicker SOI substrates, as the coupler region can support multiple (vertical) modes. In this situation, the field in the periodic device can be expressed as a linear combination of the supported Bloch modes

$$E(y,z) = \sum_i c_i \cdot \vartheta_i(y,z), \tag{6}$$

#126348 - $15.00 USD Received 1 Apr 2010; revised 16 May 2010; accepted 19 May 2010; published 1 Jul 2010

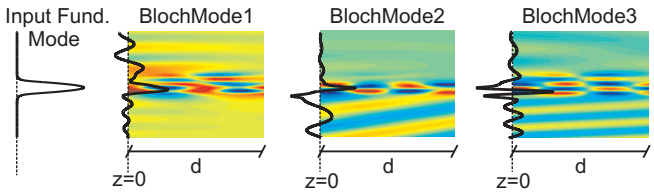

Fig. 3. Bloch modes for one grating period, their transversal profile at $z = 0$ and input fundamental mode for the grating studied in section 5.

where c_i is the complex amplitude of the i-th Bloch mode that depends on the input field launched into the grating region.

Figure 3 shows the field profiles (for one grating period) of the three lowest order Bloch modes supported by a grating with $t_w = 1.5\mu$m, $t_g = 0.75\mu$m, $d = 0.86\mu$m and $DC = 50\%$. It can be seen that each Bloch mode has a different set of air and substrate radiation beams. In general, the weighted sum of these Bloch modes (6) will result in multiple radiation beams, thus reducing coupling efficiency of the grating into a desired diffraction order.

In this paper we demonstrate that for a properly chosen input excitation the power coupled to higher order Bloch modes can be minimized, i.e. $c_1 \approx 1$ and $c_{i\neq 1} \approx 0$. Under this condition, as explained in detail in next section, the grating region is monomode. Thus, properly choosing the grating pitch, a single air radiation beam can be achieved.

4. Single mode excitation

For a given input field, the coupling to a specific Bloch mode is proportional to the matching between the excitation field and the Bloch mode profiles. The following inner product will be used to represent this field matching:

$$\langle \phi_{IN}(y), \vartheta_i(y,0) \rangle = \int \phi_{IN}(y) \cdot \vartheta_i^*(y,0) \mathrm{d}y, \tag{7}$$

where $\phi_{IN}(y)$ is the excitation field.

Effective monomode behavior of the grating will be achieved when the following condition is satisfied (see Appendix A)

$$\langle \phi_{IN}(y), \vartheta_i(y,0) \rangle \approx 0 \text{ for } i \neq 1 \tag{8}$$

In the 2D schematics shown in Fig. 2, the excitation of the grating depends on the access waveguide height (t_{aw}), since $\phi_{IN}(y)$ is the fundamental mode of this waveguide. Here we show that condition (8) can be fulfilled by optimizing t_{aw}. In Fig. 4a the inner product (7) is shown as a function of the height of the access waveguide t_{aw} for three different grating etch depths (750nm, 650nm, and 550nm). These etch depths have been chosen to fulfill the vertical single-mode condition for a $t_w = 1.5\mu$m rib waveguide [23]. From the results shown in Fig. 4a, it can be concluded that:

- Condition (8) is satisfied only for a specific height of the access waveguide.
- The optimum value for t_{aw} depends on the etch depth as

$$t_{aw}^{opt} \approx t_w - t_g. \tag{9}$$

We have verified that these conclusions remain valid for a broad range of grating pitches and duty cycles. Furthemore, the influence of wavelength of the optimal structure design, namely

#126348 - $15.00 USD Received 1 Apr 2010; revised 16 May 2010; accepted 19 May 2010; published 1 Jul 2010

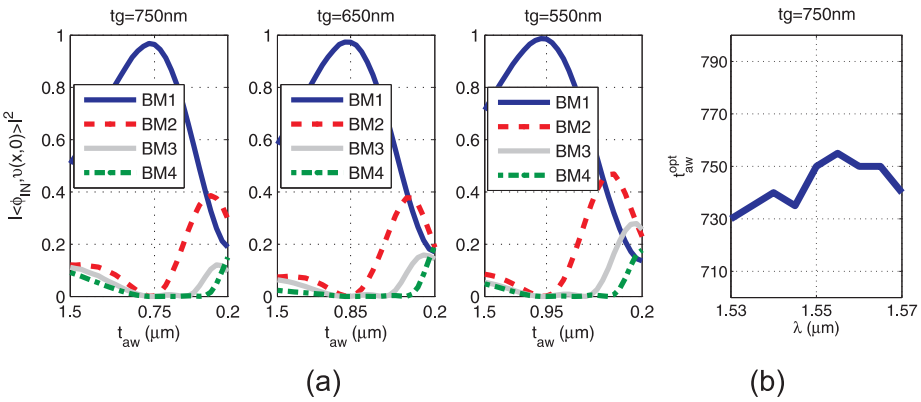

Fig. 4. (a) Inner product $|\langle \phi_{IN}, \vartheta_i \rangle|^2$ for Bloch modes BM_i for gratings with different etch depths t_g varying the access waveguide height, t_{aw}. (b) Optimum access waveguide height, t_{aw}^{opt}, as a function of wavelength, for an etch depth $t_g = 750$nm.

the access waveguide thickness, was calculated, as it is shown in Fig. 4b. It is observed that the variation of the optimal value of t_{aw} corresponding to the minimal excitation of the higher order Bloch modes is minimal, i.e. less than 25nm of the nominal design value, for the wavelength range 1530nm - 1570nm (telecom C band).

Thus the power coupled to the higher order Bloch modes can be minimized using a properly designed access waveguide. Besides, as $t_{aw}^{opt} \approx t_w - t_g$, it is an advantage of this design that the grating section can be fabricated using the same etch depth as the access waveguide and the remaining structures in the planar waveguide circuit. This is an important advantage of the proposed design, as the chip can be fabricated using standard i-line stepper lithography using a single etch depth process.

Indeed, in order to achieve the optimal excitation, the rib mode field has to be transformed into the fundamental mode of (thinner) slab waveguide. This is readily achieved using an inverse taper [29], as illustrated in Fig. 5. The inverse taper length ($\sim$1 mm, see Appendix B) is indeed significantly longer compared to inverse tapers implemented in thin silicon wire waveguides (e.g., [6], 250 nm thick SOI). This is because we implement the inverse taper concept in a comparatively thick (1.5μm) SOI ridge waveguide. In our ridge waveguide, the fundamental waveguide mode confinement is substantially reduced compared to a silicon wire waveguide. Therefore, adiabatic mode manipulation demands substantially longer taper lengths in thick SOI ridge waveguides compared to Si-wires. We compared the performance of inverse taper with a standard (conventional, not-inverse) taper. Indeed, the conventional taper can be effectively used to transform the mode laterally. However, unlike our inverse taper that performs both lateral and vertical mode transformation, the standard taper does not transform the field in the vertical direction. Such vertical mode transformation (from the ridge waveguide of height 1.5μm to a slab waveguide of height 0.75μm, see Fig. 8) is a fundamental prerequisite for avoiding excitation of higher order Bloch modes (e.g., Fig. 4). For comparison, we estimated the higher order mode excitation using a conventional taper. By calculating the mode overlap integral (Eq. 7), we found that the excitation coefficients for the 2nd, 3rd and 4th order Bloch modes are: 0.12, 0.11 and 0.09 , respectively. By using the inverse taper, these coefficients are reduced by several orders or magnitude and are next to zero for an optimal value of t_{aw} (Fig. 4). This effective mitigation of the higher-order Bloch mode excitation is the fundamental advantage of using (in our grating coupler) the inverse taper rather than the conventional taper. An added advantage of the inverse taper is a substantially reduced return loss, with the calcu-

#126348 - $15.00 USD Received 1 Apr 2010; revised 16 May 2010; accepted 19 May 2010; published 1 Jul 2010

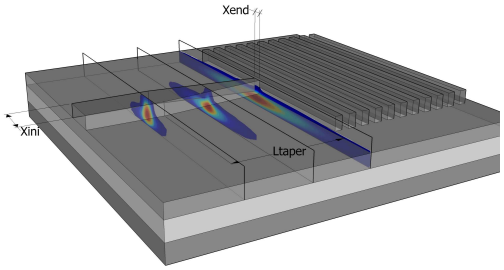

Fig. 5. Complete device 3D model including interconnection waveguide, excitation stage and grating coupler.

lated reflection at the taper-grating boundary as small as 0.16 % for the inverse taper compared to 31.6 % for conventional taper. A detailed description of the design of the taper is given in Appendix B.

Once an adequate excitation is obtained as per Eq. (9), the grating coupler can be designed using only the first Bloch mode.

5. Grating design

In this section, a systematic method of grating coupler design in a micrometric rib waveguide is presented. The proposed strategy can be divided in two parts. First, the Bloch mode analysis of the structure will be used to screen regions of interest. Subsequently for the structures belonging to these regions, the complete electromagnetical problem will be solved using the optimized access waveguide height defined in Eq. (9), choosing the one that offers the best performance.

From the Bloch mode analysis of the grating the value of the effective index (n_g), the radiation losses (α) and the reflection at the interface between the access waveguide and the grating are calculated [27, 30] and used to define the regions of interest for the grating geometry.

Knowing the effective index of the excited Bloch mode and using Eqs. (4) and (5), the number of radiating diffraction orders to the air and to the substrate and their angle of radiation is calculated as a function of the grating pitch. Regions of interest will be searched only for ranges of pitch with a single radiating diffraction order to the air.

Before defining a region of interest for the radiation loss, it has to be reminded that α accounts for air and substrate radiation. Thus information of coupling to fiber efficiency can not directly be extracted from its value. In order to define a region of interest for α the most favorable case is assumed, i.e. all the radiation goes to the air. Then the inner product between fiber mode and the exponential radiated field ($e^{-\alpha z}$) is studied as a function of α. Being the maximum theoretical value of the overlap 80% (unapodized grating)[28], a lower bound of 60% will be set, belonging to the region of interest only those structures that have a field attenuation constant $\alpha = 0.035\mathrm{Np}/\mu\mathrm{m}$ to $0.36\,\mathrm{Np}/\mu\mathrm{m}$. Points not belonging to the region of interest can be discarded.

On the other hand we set an upper bound for the reflections to the 10% of the input power.

According to the criteria above, only those structures that have only one radiating diffraction order to the air, an attenuation constant corresponding to a fiber mode overlap theoretically higher than 60% and a reflection in the interface between the access waveguide and the grating

#126348 - $15.00 USD Received 1 Apr 2010; revised 16 May 2010; accepted 19 May 2010; published 1 Jul 2010

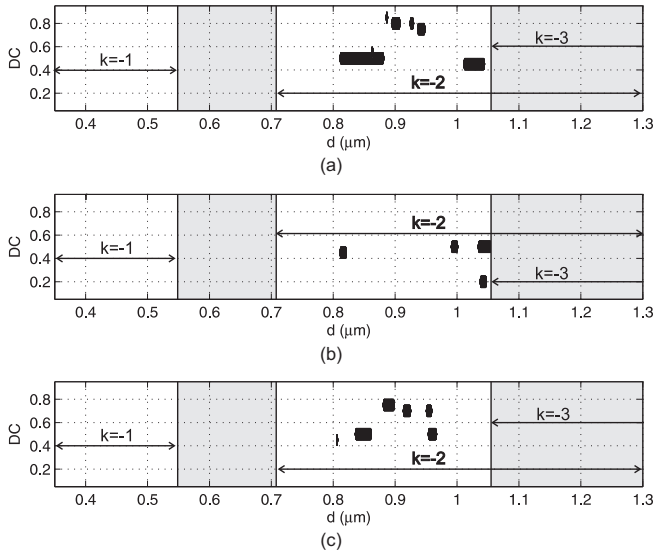

Fig. 6. Regions of interest for different etch depths: a) $t_g = 750$nm b) $t_g = 650$nm c) $t_g = 550$nm.

lower than 10% belong to the region of interest.

Once the regions of interest have been calculated, the complete elctromagnetic problem is solved only within these geometries. Input excitation is assumed to be the fundamental mode of the access waveguide. This way the actual values for radiation angle, power coupled to the fiber and back reflections are determined.

Finally the most suitable one from the analyzed structures is chosen.

This design process is applied to a grating implemented in a 1.5μm thick rib SOI waveguide, studying the regions of interest as a function of the duty cycle and pitch of the grating for three different etch depths ($t_{g1} = 750$nm, $t_{g2} = 650$nm, $t_{g3} = 550$nm) that meet the Soref's criterion [23].

In Fig. 6 the range of pitch where diffraction orders k =-1,-2,-3 can radiate are shown. The unshaded regions correspond to ranges of pitch where only one diffraction order can radiate and thus where the modal analysis is fulfilled. Black zones define the regions of interest found.

The first conclusion of this study is that the conventional coupler design using diffraction order k =-1 is not suitable in this case, as no point belonging to the region of interest has been found for the corresponding range of pitch.

The complete electromagnetical problem is solved for the regions of interest corresponding to diffraction order k =-2, being the one with $t_g = 750$nm, $d = 0.86\mu$m and $DC = 50\%$ the structure that offers the best performance.

6. Calculated results for optimal grating design

The performance of an optimized grating coupler with a length of 34.4μm, with an etch depth of $t_g = 750$nm, a pitch of $d = 0.86\mu$m, and a duty cycle of $DC = 50\%$, is discussed. An access waveguide of height $t_{aw} = 750$nm to ensure single-mode excitation is used. The results have been obtained with our in-house numerical tool [31], based on Fourier eigenmode expansion method, developed for the design of gratings. They have been verified using a commercial Finite Difference Time Domain (FDTD) tool (RSoft).

The grating radiates 88.9% of the incident power upwards, being 65.6% of the incident power

#126348 - $15.00 USD Received 1 Apr 2010; revised 16 May 2010; accepted 19 May 2010; published 1 Jul 2010

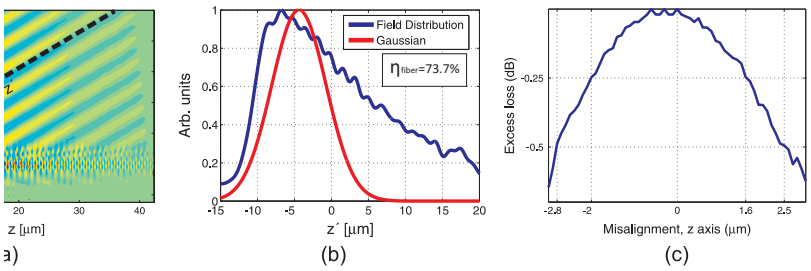

Fig. 7. (a) $|E(y,z)|$ for the proposed grating excited with an optimized access waveguide. (b) Gaussian field profile of a standard (SMF-28) optical fiber and near field distribution of the grating (cut along the dashed line shown in Fig. 7a) (c) Misalignment tolerance of the coupler (in-plane displacement).

coupled into a standard fiber. The 3dB bandwidth of the structure is $\sim$ 40nm. These results compare favorably to those obtained in grating couplers for Si-wire waveguides [12, 13, 14]. The low reflection level ($P_R = 0.163\%$) of the device is also remarkable. The angle of radiation $\theta_{-2} = -13.4\ ^\circ$ coincides with the one predicted by Eq. (4) for the diffraction order $k = -2$ of the Bloch mode with $n_{g1} = 3.37$. This is the only Bloch mode excited by the optimized access waveguide.

Figure 7a shows the modulus of the electric field when the grating is excited with the fundamental mode of the access waveguide. It can be clearly seen how a single-beam radiation is produced. Figure 7b shows the near field of the grating (a cut along the axis perpendicular to the optical fiber in the y-z plane, dashed line in Fig. 7a) calculated by the FDTD, and the Gaussian beam of standard (SMF-28) optical fiber, including the calculated mode overlap value. Furthermore, the Gaussian beam input was used to validate the concept, and the coupling efficiency to the fundamental mode of the SOI ridge waveguide was calculated by FDTD, yielding an efficiency of 65.1 % (1.86 dB). Using this approach, we also calculated the alignment tolerance of the coupler. The calculated tolerances (in-plane displacement) are shown in Fig. 7c. The 0.5 dB tolerance is estimated as 5 ($\pm$2.5) micrometers.

7. Conclusion

A grating coupler implemented in a SOI micrometric rib waveguide has been demonstrated. To achieve single-mode excitation of the grating, the use of an access waveguide with the same height as the grating etched slots is proposed, which also allows single-etch step fabrication. A systematic design process is proposed based on the use of the Bloch mode analysis. The use of a single step inverse taper reduces loss penalty between the grating and the interconnection waveguide while at the same time ensures single-mode excitation of the grating. For the optimized design, 65.6% of the injected power is coupled to an optical fiber (SMF-28) at a wavelength of $\lambda = 1.55\mu$m.

Appendix A

In this appendix we will prove the condition for monomode excitation shown in Eq. (8). Although scalar approximation (i.e. $H = Y_o E$, being H and E the magnetical and electrical mode fields and Y_o the mode admittance [32]) will be used here for simplicity, conclusions are also valid for the vectorial case. First, condition of the continuity of the tangential fields is imposed at both sides of the interface between the access waveguide and the grating. This condition, assuming the the structure is excited with the fundamental mode of the access waveguide ($\phi_{IN} = \phi_1$)

#126348 - $15.00 USD Received 1 Apr 2010; revised 16 May 2010; accepted 19 May 2010; published 1 Jul 2010

can be expressed as:

$$\phi_1 + \sum_k \rho_{1k}\phi_k = \sum_i c_i \vartheta_i(y,0) \tag{A.1}$$

$$Y^{\phi}_{o1}\phi_1 - \sum_k \rho_{1k} Y^{\phi}_{ok}\phi_k = \sum_i c_i Y^{\vartheta}_{oi}\vartheta_i(y,0) \tag{A.2}$$

where ϕ_k are the modes of the access waveguide, $\vartheta_i(y,0)$ are the transverse cuts of the Bloch modes of the grating at the interface ($z=0$) between the access waveguide and the grating, ρ_{1k} is the reflection coefficient for the access waveguide modes, Y^{ϕ}_{ok}, Y^{ϑ}_{oi} are the admittances of the modes of the access waveguide and grating respectively, and c_i are the excitation coefficients.

Applying the mode matching method, i.e., multiplying Eq. (A.1) by $\vartheta_i(y,0)$, Eq. (A.2) by ϕ_k and integrating, the excitation and reflection coefficients are obtained:

$$c_i = \langle \phi_1, \vartheta_i(y,0)\rangle (1+\rho_{11}) + \sum_{k\neq 1} \rho_{1k} \langle \phi_k, \vartheta_i(y,0)\rangle \tag{A.3}$$

$$\rho_{1k} = \langle \phi_k, \phi_1\rangle \frac{Y^{\phi}_{o1}}{Y^{\phi}_{ok}} - \sum_k c_i \langle \phi_k, \vartheta_i(x,0)\rangle \frac{Y^{\vartheta}_{oi}}{Y^{\phi}_{ok}} \tag{A.4}$$

If the cross-correlation between the modes of the access waveguide and the grating is negligible

$$\langle \phi_k, \vartheta_i(y,0)\rangle \approx 0 \;\; k \neq i \tag{A.5}$$

and taking into account that $\phi_{IN} = \phi_1$ expressions (A.3) and (A.4) can be approximated as

$$\begin{aligned} c_1 &\approx \langle \phi_{IN}, \vartheta_1(y,0)\rangle (1+\rho_{11}) \\ c_{i\neq 1} &\approx 0 \end{aligned} \tag{A.6}$$

$$\rho_{11} \approx \frac{Y^{\phi}_{o1} - \langle \phi_{IN}, \vartheta_1\rangle^2 Y^{\vartheta}_{o1}}{Y^{\phi}_{o1} + \langle \phi_{IN}, \vartheta_1\rangle^2 Y^{\vartheta}_{o1}}. \tag{A.7}$$

Equation (A.6) shows that only first Bloch mode is excited when condition (A.5) is fulfilled. On the other hand when the correlation $\langle \phi_{IN}, \vartheta_1(y,0)\rangle$ is close to unity and being far from the Bragg condition the reflection coefficient (ρ_{11}) is negligible.

Appendix B

In this section the use of an inverse taper is proposed for the transition between the interconnection waveguide and the grating, including a systematic design process.

The interconnection waveguides are designed to operate in single-mode regime, their dimensions and the field profile of the mode are shown in Fig. 8a. The purpose of the excitation stage is to adiabatically make the transition between this mode and an objective field profile. In order to maximize the performance of the grating, according to the discussion in section 4, two conditions can be defined for the excitation field profile:

- Field distribution along the y-axis has to ensure single-mode excitation of the grating region.

#126348 - $15.00 USD Received 1 Apr 2010; revised 16 May 2010; accepted 19 May 2010; published 1 Jul 2010

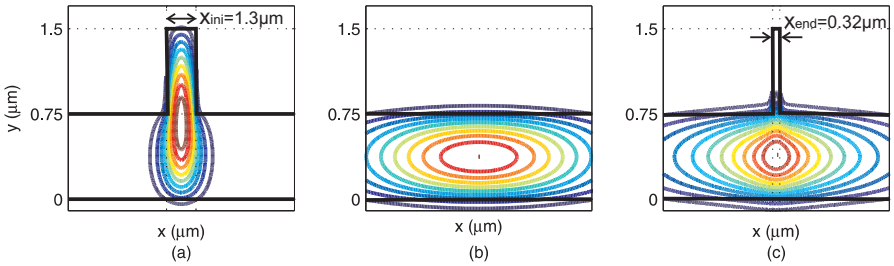

Fig. 8. (a) Interconnection rib waveguide and fundamental mode (b) Objective field (c) Rib waveguide at the end of inverse taper and fundamental mode.

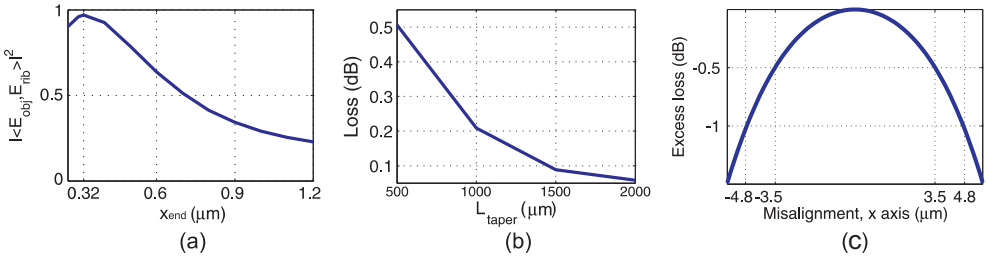

Fig. 9. (a) Inner product for objective field (E_{obj}) and excitation field (E_{rib}) for inversely tapered rib of width x_{end} (b) Loss of the inverse taper as a function of taper length L_{taper} (c) Alignment tolerance between the grating coupler and the inverse taper.

- Field distribution along the x-axis has to maximize the overlap with a near-Gaussian field of the optical fiber mode.

Thereby, an objective field distribution can be defined as:

$$E_{obj}(x,y) = E(x)E(y), \tag{B.1}$$

where $E(x)$ is a Gaussian function, and $E(y)$ is the x-polarized fundamental mode of a slab waveguide with a height that ensures single-mode excitation, as discussed in section 4. The objective field profile calculated for our grating design (section 5) is shown in Fig. 8.

Thus, in order to maximize the mode match with the objective field, the inner product is studied for different values of the rib width, as shown in Fig. 9a. The optimum value for the taper tip width is found to be $x_{end} = 0.32\mu$m, which can be fabricated using i-line stepper lithography.

Figure 9b plots the loss of the taper as a function of its length. Insertion losses below 0.2dB can be achieved for taper lengths greater than 1000μm. Finally in Fig. 9c the alignment tolerance between the grating and the inverse taper was calculated. It was found that our coupler design is robust to this misalignment, with a 0.5 dB tolerance of 7 ($\pm$3.5) micrometers.

Acknowledgments

This work was supported in part by the Spanish Ministry of Science and Innovation under Project TEC2009-10152, by the Andalusian Regional Ministry of Science, Innovation and Business (CICYE) under Excellence Research Project P07-TIC-02946 and by the project AVANZA I+D (Celtic) TSI-020400-2008.

#126348 - $15.00 USD Received 1 Apr 2010; revised 16 May 2010; accepted 19 May 2010; published 1 Jul 2010